Carbohydrate Polymers 317 (2023) 121085

Contents lists available at ScienceDirect

Carbohydrate Polymers

journal homepage: www.elsevier.com/locate/carbpol

20(R)-ginsenoside Rg3-loaded polyurethane/marine polysaccharide based nanofiber dressings improved burn wound healing potentials

Xiong Guo [a,1], Fangfang Xiu [a,1], Hriday Bera [a,e], Yasir Faraz Abbasi [a], Yang Chen [a], Liangwei Si [a], Peixin Liu [a], Chunwei Zhao [a], Xing Tang [b], Yu Feng [a], Dongmei Cun [a,*], Xia Zhao [c], Mingshi Yang [a,d,**]

[a] Wuya College of Innovation, Shenyang Pharmaceutical University, Shenyang l10016, China
[b] Department of Pharmaceutics, School of Pharmacy, Shenyang Pharmaceutical University, Shenyang 110016, China
[c] Key Laboratory of Marine Drugs, Ministry of Education, Shandong Provincial Key Laboratory of Glycoscience and Glycoengineering, School of Medicine and Pharmacy, Ocean University of China, Qingdao 266003, China
[d] Department of Pharmacy, Faculty of Health and Medical Sciences, University of Copenhagen, Universitetsparken 2, DK-2100 Copenhagen, Denmark
[e] Roy College of Pharmacy & Allied Health Sciences, Durgapur, West Bengal, 713206, India

ARTICLE INFO

Keywords:
Hydroxypropyl trimethyl ammonium chloride chitosan
Sodium alginate
Polyurethane
Nanofibrous scaffolds
Ginsenoside
Third-degree burn

ABSTRACT

The management of deep burn injuries is extremely challenging, ascribed to their delayed wound healing rate, susceptibility for bacterial infections, pain, and increased risk of hypertrophic scarring. In our current investigation, a series of composite nanofiber dressings (NFDs) based on polyurethane (PU) and marine polysaccharides (*i.e.,* hydroxypropyl trimethyl ammonium chloride chitosan, HACC and sodium alginate, SA) were accomplished by electrospinning and freeze-drying protocols. The 20(*R*)-ginsenoside Rg3 (Rg3) was further loaded into these NFDs to inhibit the formation of excessive wound scars. The PU/HACC/SA/Rg3 dressings showed a sandwich-like structure. The Rg3 was encapsulated in the middle layers of these NFDs and slowly released over 30 days. The PU/HACC/SA and PU/HACC/SA/Rg3 composite dressings demonstrated superior wound healing potentials over other NFDs. These dressings also displayed favorable cytocompatibility with keratinocytes and fibroblasts and could dramatically accelerate epidermal wound closure rate following 21 days of the treatment of a deep burn wound animal model. Interestingly, the PU/HACC/SA/Rg3 obviously reduced the excessive scar formation, with a collagen type I/III ratio closer to the normal skin. Overall, this study represented PU/HACC/SA/Rg3 as a promising multifunctional wound dressing, which promoted the regeneration of burn skins and attenuated scar formation.

1. Introduction

A burn wound is one of the most common and devastating skin injuries, causing serious morbidity and enormous financial burdens among the burn survivors (Wang et al., 2018). Based on the depth of the skin damage, burn injuries could be classified into three categories. The first-degree burns could only reach the epidermal layers, leaving redness. The deep dermal (second degree) burns could affect the middle layers of the skin and result in the formation of blisters, exudates, and excessive scars during healing. The third-degree burn wounds cause severe injuries, which are extremely difficult to heal owing to the destruction of nearly all of the skin layers (Khan et al., 2020). To promote the healing of third-degree burn wounds, skin substitutes are often required to cover the wound to avoid bacterial infections and to regulate the wound microenvironment. However, the patients with deep burn injuries would always lack sufficient skin donors and require appropriate wound dressings as skin equivalent substitutes (Atiyeh et al., 2005). Nowadays a variety of wound dressings, including films, hydrocolloids, foams, and hydrogels, *etc.* are available on the market (Gupta et al., 2019). Among these scaffolds, nanofiber dressings (NFDs)

* Corresponding author at: Wuya College of Innovation, Shenyang Pharmaceutical University, Shenyang l10016, China
** Corresponding author at: Wuya College of Innovation, Shenyang Pharmaceutical University, Shenyang l10016, China; Department of Pharmacy, Faculty of Health and Medical Sciences, University of Copenhagen, Universitetsparken 2, DK-2100 Copenhagen, Denmark.
E-mail addresses: cundongmei@163.com (D. Cun), mingshi.yang@sund.ku.dk (M. Yang).
[1] These authors contributed equally to this work.

https://doi.org/10.1016/j.carbpol.2023.121085
Received 29 December 2022; Received in revised form 26 May 2023; Accepted 30 May 2023
Available online 1 June 2023

have attracted overwhelming attention in recent years due to their unique properties such as high surface area, nano-porosity, and the extracellular matrix (ECM) mimicking architectures. Eventually, these are widely employed as promising dressings for treating deep burn wounds (Farokhi et al., 2018). To fabricate NFDs, electrospinning protocol can be a promising method due to its adaptability, cost-effectiveness, and scalability (Dos Santos et al., 2020). An array of synthetic polymers with outstanding mechanical properties, such as polyurethane (PU), poly(lactide-*co*-glycolide) (PLGA), and polylactic acid (PLA) has been used to construct NFDs (Noor et al., 2022). Among these synthetic polymers, PU has frequently been employed in the development of NFDs owing to its superior barrier properties and oxygen permeability (Unnithan et al., 2012). The PU-based NFDs are also very elastic and flexible. Over the years, several pioneering research groups developed multifunctional PU based NFDs primarily to overcome numerous challenges during the healing process of deep burn injuries like increased wound exudate, susceptibility to bacterial infections, poor wound healing rate, and hypertrophic scarring (Noor et al., 2022). To accomplish multifunctional NFDs, various marine polysaccharides with inherent therapeutic properties are often integrated with NFDs, which could significantly promote the third-degree burn wound healing process (Iacob et al., 2020). Chitosan (CS) is an amino-polysaccharide extracted from marine crustaceans crabs and displays an ability to form polyelectrolyte complexes with negatively charged macromolecules. The CS-derived biomaterials have received considerable interest due to their biocompatibility, biodegradability, and antimicrobial properties (Periayah et al., 2016). However, the applications of CS are restricted due to its inherent poor solubility in alkaline media (> pH 6.5). Different chemical modification approaches, such as carboxylation, quaternization, acylation, PEGylation, *etc.* could improve the aqueous solubility and biological properties of CS (Periayah et al., 2016). Among several CS derivatives, chitosan quaternary ammonium salt (hydroxypropyl trimethyl ammonium chloride chitosan, HACC) demonstrates outstanding aqueous solubility and enhanced antimicrobial properties, which make it appropriate for deep burn wound therapy (Min et al., 2020). However, it has been reported that the antibacterial potentials of HACC could be enhanced with an increase in its substitution degrees, causing higher cytotoxicity (Peng et al., 2010). To overcome such shortfalls, sodium alginate (SA), a naturally occurring anionic polysaccharide obtained from brown seaweed, could be doped with cationic HACC to reduce its cytotoxicity (Borges et al., 2006). SA is a safe polysaccharide with negligible cytotoxicity. It has widely been investigated as wound dressing material ascribed to its biocompatibility and excellent moisture retention ability. The SA gels could also portray structural configuration similar to the extracellular matrices of the tissues (K. Y. Lee & Mooney, 2012). The combined advantages of HACC and SA could effectively promote deep burn wound healing and resolve numerous difficulties faced during the healing process. For instance, the cationic HACC could exert antibacterial activities to prevent wound infections, while anionic SA chains could absorb wound exudates, regulate the wound healing micro-environments and interact with cationic HACC residues to reduce their cytotoxicity (Borges et al., 2006). However, the electrospinning of SA to produce nanofibers is still extremely challenging as its gelation occurs at a very low concentration, and SA is insoluble in the most organic solvents (Moon et al., 2009). Thus, the SA could be integrated with the electrospun nanofibrous scaffolds by adopting special preparatory techniques such as freeze-drying, yielding composite NFDs (Y. Li et al., 2021). Freeze-drying is a commonly used post-treatment technique to enhance the physical properties and stability of the electrospun fibers (Aghmiuni et al., 2021). Incorporation of the freeze-drying process might increase the complexity and costs of the NFDs preparation. However, freeze-drying could assist in removing residual organic solvent from the electrospun fibers and providing porous structure in the dressings, which would promote the rapid absorption of wound exudate and regulate the local moist environment of the wound.

In recent years, various therapeutically active agents were loaded within the NFDs to achieve improved wound healing outcomes (Sofi et al., 2020). 20(*R*)-ginsenoside Rg3 (Rg3) is the most famous component extracted from red ginseng (*Panax ginseng*) and exhibits important pharmacological actions, including anti-cancer, immunomodulation, and antioxidative activities (L. Li et al., 2020). Studies indicated that Rg3 could inhibit keloid fibroblast migration by upregulation the expression of anti-fibrotic genes, such as interferon (INF-γ) and transforming growth factor (TGF-β3), while decreasing the expression of profibrotic genes like α-smooth muscle actin (α-SMA) and connective-tissue growth factor (Tang et al., 2018). These findings suggested that Rg3 might be a potential therapy for the inhibition of hypertrophic scar formation. When loaded into the NFDs, Rg3 could be slowly eluted out and control the rate of extracellular matrix regeneration, preventing hypertrophic scarring (Sun et al., 2014). Thus, Rg3-loaded PU/HACC/SA based multifunctional NFDs could be strategically fabricated as burn wound healing scaffolds, which has not yet been explored by any research groups.

To fulfill the research gaps, we hypothesized that the Rg3-loaded PU/HACC/SA based NFDs would demonstrate favorable morphological and physicochemical properties, promote the healing of third-degree burn wounds and prevent the hypertrophic scar formation. The primary objectives of the current research endeavors were to accomplish PU/HACC/SA/Rg3 based multifunctional NFDs through electrospinning coupled freeze-drying technology. The Rg3, PU and HACC were blended to prepare composite nanofibrous mats, which were subsequently immersed in a SA aqueous solution and freeze-dried to construct multifunctional PU/HACC/SA/Rg3 based NFDs. Furthermore, their enhanced deep burn wound healing potentials over other control composite scaffolds were examined through various *in vitro* and *in vivo* investigations.

2. Experimental section

2.1. Materials

PU (HP-93A-100) was obtained as a gift from Lubrizol Advanced Materials (Shanghai, China). A free sample of SA (viscosity 80 mPa·s, M/G = 6/4) was provided by the Qingdao Gather Great Ocean Algae Group (Qingdao, China). HACC (Mw = 91.8 kDa) was obtained from the Marine Biomedical Research Institute of Qingdao (Qingdao, China), and its degree of quaternization (DQ) was 95.1 % (determined by titrating the amount of Cl^- ions on the HACC using the Volhard method). Rg3 (Macklin, China), keratinocytes (HaCat, Shanghai Biowing Applied Biotechnology, China), fibroblasts (NIH-3T3, General Hospital of Northern Theater Command, Shenyang, China), cell counting kit-8 (CCK-8, Saiwen innovation Biotechnology, China), hexafluoroisopropanol (HFIP, Macklin, China), α-MEM culture medium (Hyclone, LoganUtah, USA), DMEM medium (Meilunbio, China), and SORBALGON® microfiber dressings (Paul Hartmann AG, Germany) were used.

2.2. Characterization of HACC and SA

2.2.1. Gel Permeation Chromatography (GPC) method

The number average molecular weight (Mn) and weight average molecular weight (Mw) values of HACC and SA were determined by a GPC instrument (LC20 Shimadzu) equipped with a TSKgel GMPWXL column. The GPC analysis was performed with a flow rate of 0.6 $mL{\cdot}min^{-1}$, injection volume 20 μL, and column temperature thermostat 35 °C. The eluent was monitored by a refractive index detector of optical unit temperature 25 °C and peak width 0.1 min. The molecular weights were determined from the calibration curve with polyethylene oxide standards (500–500,000). Đ was calculated using the formula: Đ = Mw/Mn.

2.2.2. ^1H NMR spectra

^1H NMR spectra of HACC and SA were recorded on a 600 MHz Avance NEO spectrometer (Bruker, USA) at 25 °C. HACC was dissolved in 0.1 % DCl/D_2O at a concentration of 10 mg•mL^{-1}. SA was dissolved in D_2O with a concentration of 10 mg•mL^{-1}.

2.3. Fabrication of multifunctional NFDs

2.3.1. Formulation of pure PU and PU/HACC based NFDs

The PU/HACC based NFDs were fabricated following a previously published protocol (Unnithan et al., 2012). Briefly, variable mass ratios of PU and HACC were dissolved in HFIP and the resulting solutions were loaded into a 5.0 mL syringe. The electrospinning process was then carried out using an electrospinner (Ucalery, Beijing, China) under a controlled environment (25 ± 2 °C and relative humidity, 20 ± 5 %). The feeding rate of the solutions was set at 1.0–3.0 mL•h^{-1}. The high electrical voltage of 18–24 kV was applied at a regular distance of 15 cm from the needle tip to the collector. The PU/HACC nanofiber mats were subsequently vacuum dried at 25 °C for 48 h to further evaporate the solvent. Pure PU based NFDs were also prepared adopting analogous methodology without introducing HACC into the spinning solution.

2.3.2. Preparation of PU/SA and PU/HACC/SA based NFDs

The pure PU and PU/HACC based nanofiber films were cut into round shapes and suspended in aqueous SA solutions (1.0 %, w/w). These were pre-frozen at −80 °C for 1 h and transferred to a freeze-dryer (SCIENTZ-12N, Ningbo, China) for 48 h to obtain PU/SA and PU/HACC/SA based composite dressings.

2.3.3. Preparation of Rg3 loaded PU/HACC/SA NFDs

An accurately measured quantities of Rg3, PU, and HACC was completely dissolved in HFIP to produce the spinning solutions (Sun et al., 2014). After electrospinning, the nanofiber mats were peeled off from the receiving paper and the residual solvent was removed. These mats were cut into circles (diameter, 5.0 cm), suspended in 1.0 % aqueous SA solution, pre-frozen and placed in a freeze dryer for 48 h to yield PU/HACC/SA/Rg3 dressings.

2.4. Morphology of NFDs

The surface and cross-sectional morphologies of various NFDs were analyzed under a field emission scanning electron microscopy (SEM, Gemini 300, Zeiss, Germany) with a secondary-electron detector and an acceleration voltage of 12 kV. The samples were fixed on the metal stubs attached to double-sided adhesive tapes and were gold coated (5–10 nm) under an argon atmosphere. The average fiber diameters of NFDs were measured using NIH ImageJ software (National Institutes of Health, Bethesda, MD) considering >100 randomly selected fibers in the images.

2.5. Mechanical properties

The NFDs were cut into long strips (1.0 cm × 2.0 cm) and their thicknesses were measured using an electronic micrometer (Nscing Es, China). The mechanical properties of the NFDs including tensile strength, modulus and elongation were tested using a Texture Analyzer (CT-3/4500, Brookfield, USA). The NFDs were stretched at a speed of 0.5 mm•S^{-1} until peeled off finally at room temperature.

2.6. Water absorption rates

The water absorption rates (WARs) of NFDs were assessed by adopting gravimetric method (Porrelli et al., 2021). Precisely, the NFDs were cut into small pieces (1.0 × 1.0 cm), weighed (W_{dry}) and placed in a dish. The PBS (pH 7.4) was added dropwise to their surfaces until the exudation appeared and waited for 30 min. The excess surface liquid was then gently wiped off using filter paper before weighing NFDs (W_{wet}). The WARs were subsequently estimated using the following expression:

$$\mathrm{WAR}\ (\%) = W_{wet} - W_{dry}/W_{dry} \times 100\%$$

2.7. Water vapor transmission rates

The water vapor transmission rates (WVTRs) of NFDs were measured using the reported protocol (Tarusha et al., 2018). Briefly, the round-shaped NFDs (diameter,3.0 cm) were attached to the mouth of a glass vial containing 4.0 mL of pure water. The bottles were weighed before being placed in a monitored chamber (CIMO, China) at 37 °C with 50 % relative humidity. The weights of these bottles were further measured after 24 h incubation. The WVTRs were then determined based on the following equation:

$$\mathrm{WVTR}\ \left(g \bullet m^{-2} \bullet day^{-1}\right) = \Delta m/\Delta t \times A$$

The Δm denotes the lost weight (g), Δt refers to the time, and A represents the area of NFDs exposed to the moisture transfer (m^2).

2.8. Wettability analyses

The water contact angles (WCAs) of the NFDs were determined utilizing a contact angle goniometer (SINDIN, China). A drop of pure water (10 μL) was added onto the surfaces of the NFDs. The changes of WCAs over time were tracked and the data were analyzed using NIH Image J software.

2.9. Release study

The *in vitro* release patterns of Rg3 from the NFDs were examined in the phosphate buffer saline (PBS, pH 7.4) solution containing 30 % (v/v) methanol and 0.02 % (w/v) sodium azide (Aoyagi et al., 2007). The composite dressings (~10.0 mg) were placed in a centrifuge tube with 4.0 mL medium and were horizontally agitated at 100 rpm. At designated time points (0.5–35 days), aliquots (1.0 mL) were withdrawn and the fresh release medium was reintroduced. The Rg3 contents in these samples were analyzed according to the HPLC method reported previously (Sun et al., 2014).

2.10. Proliferation of fibroblasts and keratinocytes

The effects of different NFDs on HaCat and NIH-3T3 cell proliferation were tested by the cell counting Kit-8 (CCK-8) assay method (Bagheri et al., 2022). Prior to the investigation, various NFDs were continuously soaked in 5.0 mL of culture media for 7 days to obtain their leachates, which were then filtered through 0.22 μm sterile filters and stored at 4 °C for further uses. The fibroblasts and keratinocytes were cultured in α-MEM culture medium (Meilunbio, China) and DMEM culture medium (Meilunbio, China), respectively. Both media were supplemented with 10 % fetal bovin serum (FBS, Gibco) and 1 % penicillin-streptomycin. Subsequently, the HaCat and NIH-3T3 cells were seeded in 96-well plates at a density of 3×10^3 and 4×10^3 cells/well, respectively, and incubated in a CO_2 incubator (Thermo Scientific, USA) at 37 °C for 24 h. The old media were then discarded, replaced with fresh media containing leachates (0.5 %, 1 %, and 2 % *v*/v). Following 48 h of incubation, the cells were treated with CCK-8 reagent (APExBIO, USA) for 40 min and their optical densities (OD) were measured at 570 nm using a microplate reader (BMG LABTECH, Germany). The cell viability was then estimated based on the following formula, with non-treated cells serving as the control group.

$$\text{Cell viability}\ (\%) = OD_{test}/OD_{control} \times 100\%.$$

2.11. Migration of HaCat and NIH-3T3 cells

The scratch test was used to assess the cells migration according to the reported protocol (Alvarez et al., 2021). Briefly, HaCat and NIH-3T3 cells were seeded in a 12-well plate (5×10^4 cells/well) and allowed to grow until these reached to 80 % confluence (~24 h). Two linear scratches were created in the wells using a 200 μL plastic tip and gently washed with PBS three times to remove the cellular debris. Subsequently, the cells were treated with medium containing 1 % NFD leachates and incubated for 24 h and 48 h. The cell migration was then monitored using an optical microscope (IX81, Olympus, Japan).

2.12. Animal experiments

2.12.1. Third-degree burn wound healing efficiency

The third-degree burn wound rat model was established following protocol reported elsewhere (Guo et al., 2020). The experimental methodology was reviewed and approved by the animal ethical committee, Shenyang Pharmaceutical University, China (SYPU-IACUE-C2018−12−26−202). Precisely, Sprague-Dawley (SD) male rats (200 ± 10 g) were anesthetized with chloral hydrate. The curved metal punch (379.94 mm^2) of desktop super temperature control scalder (YLS-5Q, China) was heated at 80 °C and tightly pressed at 10 kPa on the shaved skin of the rats' back for 18 s to create third-degree burn injuries. After 2 h, the dead skin was surgically removed with a scissor and a silicone ring was attached around the wounds utilizing special bio-glue (Gold Elephant, China) to avoid early wound contraction. The animals were randomly divided into 6 groups ($n = 12$) and treated with blank control (without dressings), positive control (Sorbalgon®) and several NFDs (*viz.,* PU/HACC, PU/SA, PU/HACC/SA and PU/HACC/SA/Rg3). The dressings were fixed onto the burn wounds of animals with elastic bandages and the rats were housed alone at 25 °C. Gentamicin sulfate was added to the animals' drinking water (0.15 g / L) for 14 days and the cage cleanliness was carefully maintained throughout the experiment to avoid bacterial infections. Every 7 days, the dressings were changed, and they were moistened with sterile saline before being changed. The body weights of rats were also monitored every day to examine their health conditions. The wound sizes of the control and various NFDs treated groups were measured by capturing pictures at several time points (7, 14 and 21 days) and the wound closure rates were assessed *via* Image J software (National Institute of Health, USA). At the end of 7th, 14th, and 21th days, different groups of animals ($n \geq 3$) were sacrificed and their wound tissues were collected for further analyses.

2.12.2. H&E and Masson's trichrome staining

The skin specimens collected at regular time intervals were fixed in 10 % formalin solution before being embedded in paraffin. The H&E and Masson's trichrome staining were then performed according to the published protocols (H. Li, Ziemer, et al., 2022; GU et al., 2022) and the representative sections were captured using an optical microscope (Olympus digital camera, Olympus, Japan).

2.12.3. Sirius red staining

The Sirius red staining of the skin tissues was performed based on previously described procedure (Castleberry et al., 2016). The tissue sections were stained with Biebrich scarlet solution (pH 9.5) for 8 min. The slices were then dehydrated, transparentized, sealed with neutral gum, and observed under polarized light microscopy (Leica DM2700P, Germany). The ratios of collagen I/III deposition were evaluated using Image Pro Plus software (version 6.0).

2.12.4. Immunofluorescence staining

The immunofluorescence staining of the skin tissues was carried out according to the reported literature (Luo et al., 2021). Precisely, the paraffin-embedded tissue sections were incubated overnight at 4 °C with anti-α-SMA (1:200, Proteintech, USA) and anti-CD31 (1:200, Proteintech, USA). The sections were then treated with Cy3-conjugated anti-rat IgG (1:300, Servicebio, China) and FITC-conjugated anti-rat IgG (1:300, Servicebio, China) for 50 min. Finally, these samples were stained with DAPI for 10 min and analyzed under a fluorescence microscope (Nikon Eclipse Ci H600L, Japan).

2.13. Statistical analyses

All experimental data were expressed as mean ± standard deviation (SD). To compare data of different groups, a one-way ANOVA with Bonferroni's multiple comparison tests was performed using the SPSS software (version 19.0, International Business Machines Corp., USA). A p value below 0.05 was regarded as statistically significant.

3. Results and discussion

3.1. Characterization of the HACC and SA

The structure of HACC and SA were shown in Fig. S1. Values of average molecular weight (Mw), number-average molecular weight (Mn), and molecular-weight dispersity (Đ, Mw/Mn) of these polysaccharides were demonstrated in Table S1. Due to size-exclusion chromatography (SEC) combined with calibration using PEO as a standard to determine apparent molecular weights, the molar masses of HACC or SA might be overestimated to a factor 4–6 (Ulset et al., 2014). The structures of the HACC and SA polysaccharides were confirmed by ^{1}H NMR (Fig. S2). Specifically, the spectrum of HACC revealed a very strong peak at 3.2 ppm of three methyl groups (-CH3) in a trimethyl quaternary ammonium fragment (Fan et al., 2021). Furthermore, the DQ of HACC was estimated by the ^{1}H NMR analysis to be 94.4 %. In ^{1}H NMR spectra of SA, multiple peaks within the range of 3.7 to 5.0 ppm were observed, which could be attributed to the protons of methine groups of hexuronic acid moieties from the SA main chain (Zheng et al., 2014).

3.2. Fabrication of multifunctional NFDs and their morphological appearances

In the present study, we were interested in fabricating HACC and SA blended PU based multifunctional NFDs. In this milieu, only HFIP could completely dissolve PU and HACC and yield clear and transparent spinning solutions, while other organic solvents, such as chloroform, DMSO and *N*, *N*-dimethylformamide failed to achieve such goal. Therefore, HFIP was chosen as the solvent in our study. Furthermore, the suitability of the total solid contents and different mass ratios of PU and HACC for the electrospinning process was investigated using a 20 G needle, a constant electric field of 15 kV and a spinning liquid flow rate of 2.0 $mL \bullet h^{-1}$. The surface morphologies of the PU/HACC based NFDs with total solid contents of 2 % portrayed bead-free homogeneous nanofibers with smooth surfaces (Fig. S3A). As the total solid content was increased from 2 % to 4 % (w/w), the conductivity of the spinning solution was enhanced and the electrospinning process was improved (Table S2), which consequently generated smooth and flat nanofibrous mats. The fiber diameters were also increased as the total solid content was raised from 2 % to 4 % (Fig. S3B). This result was consistent with the recently reported findings (Miranda et al., 2022). A further increase in the total solid content (≥6.0 %) reduced the fluidity of the spinning liquid, caused needle plugging and eventually hindered their electrospinability. Therefore, the total solids content of 4 % was selected as the optimal concentration. When the PU/HACC ratio was elevated from 1:1 to 3:1 at the same solid content (*i.e.,* 4 %), the conductivity of the spinning solution was decreased and the nanofiber diameter distribution became wider with bifurcation phenomenon (Fig. S3B). This could be attributed to the fact that HACC, as an ionizable polymer, significantly augmented the conductivity of the spinning solutions, causing superior stretching of the jets during the electrospinning process (Alipour et al., 2009). In order to ensure a proper electrospinability for the fabrication

of composite NFDs containing a higher amount of HACC, the mass ratio of PU and HACC of 2: 1 was chosen. The average nano-fiber diameter of the resulting NFDs was 177 ± 66 nm with a narrow diameter distribution.

The optimal PU/HACC NFDs were further accomplished under different conditions varying the spinning needle's inner diameter (0.40–0.9 mm), voltage (9–18 kV) and flow rates of the spinning liquid (1.0–3.0 mL•h^{-1}) and their morphologies were compared. As compared to the 18 G needle (inner diameter, 0.90 mm), the 20 G needle (inner diameter, 0.60 mm) produced thinner nanofibers with a narrower diameter distribution (Fig. S4). When the needle inner diameter was decreased, a smaller Tayler cone could form and effectively reduce the critical voltage for the jet excitation, which could efficiently stretch the jets (Xiong et al., 2021). However, while the spinning needle's inner diameter was smaller than 0.40 mm, the preparation efficiency of the nano-fibers was dramatically reduced. On the other hand, when the applied voltage was increased from 18 kV to 24 kV, both the nanofiber diameter and adhesion abilities between the fibers were decreased, but the diameter distribution was slightly broadened (Fig. S5). An enhanced voltage might supply a greater electrostatic force to scatter the spinning solutions, allowing the nano-fibers sufficiently stretched (Guo et al., 2020). However, the electrospinning instrument became unstable as the voltages higher than 24 kV, hampering the continuous NFDs production. Lastly, as the flow rate of the spinning solutions was increased from 1.0 to 3.0 mL•h^{-1}, the nano-fibers became smooth with a uniform diameter distribution. The nano-fiber diameter distribution became wider and the liquid dropping phenomenon was observed when the flow rate of the spinning liquid was further raised (Fig. S6). According to these results, the target NFDs with acceptable morphological characteristics were afforded using 20 G needle, applied voltage of 21 kV, and flow rate of 2.0 mL•h^{-1}.

An attempt was further made to fabricate PU/SA composite dressings by electrospinning combined with freeze-drying technology (Fig. S7). When a diluted SA aqueous solution (0.5 %) was applied, SA could not be uniformly distributed on the surfaces of the fibrous mats. In contrast, a 1.0 % SA solution could evenly and tightly adhere onto the surfaces of the PU fiber films. As SA concentration was further elevated to 2.0 %, the structure of the resulting NFDs became unstable, in which SA layers adhering to the surfaces of the fiber mats were likely to fall off. Therefore, a 1.0 % SA aqueous solution was selected for the preparation of PU/SA and PU/HACC/SA based composite NFDs.

The final NFDs afforded under optimal parameters were white, flat, and uniform in appearances (Fig. 1). The surface and cross-sectional microstructures of these NFDs were variable. For instance, the pure PU based NFDs (4.0 %, w/v) showed smooth fiber surfaces, absence of beads and larger fiber diameters. The cross-sectional views of PU based NFDs illustrated porous architectures within the laminated nano-fibers. The surface morphologies of the PU/SA based NFDs were relatively dense as the pores between the fibers were filled with the lyophilized SA. Their cross-sectional outlooks revealed a "sandwich" construction, where the up and down denser layers of lyophilized SA residues accommodated the middle layer of PU fibrous mat. The structures of the PU/HACC/SA base NFDs resembled to that of the PU/SA composite dressings. The cross-sectional morphologies of PU/HACC/SA scaffolds demonstrated an obvious adhesion of SA chains with the internal fibers due to their electrostatic interactions with the dissolved HACC. The surface morphologies of drug loaded NFDs (*viz.*, PU/HACC/SA/Rg3–2 % and PU/HACC/SA/Rg3–4 %) showed dense surfaces with no pores. Their cross-sectional views depicted upper and lower layers of freeze-dried SA chains and a middle layer of Rg3-loaded PU/HACC nanofiber films. The inter-fiber adhesion of these NFDs was attributed to the stronger interactions between the dissolved HACC and immersed SA segments of the top and bottom layers.

3.3. Mechanical properties

As compared to the pure PU based NFDs, various composite NFDs containing polysaccharides displayed different mechanical properties (Fig. 2A). Pristine PU based NFDs were soft and flexible in nature and their elongation ratio, tensile strength, and Young's modulus were of 331.98 % ± 23.73 %, 10.40 ± 1.49 MPa and 3.56 ± 0.22 MPa, respectively. Although it had a high elongation, it was not sticky, easy to cut and apply in the wound. The elongation ratio of PU/HACC based NFDs significantly declined ($p < 0.05$), whereas their Young's modulus notably increased relative to PU based NFDs. On the other hand, PU/SA base NFDs conferred obviously decreased tensile strength, and Young's modulus as compared to PU based NFDs ($p < 0.05$). Interestingly, the multi-layer PU/HACC/SA based NFDs displayed a considerably lower elongation ratio than that of the PU/HACC based NFDs ($p < 0.05$), but their tensile strength was remarkably higher than that of the PU/SA based NFDs ($p < 0.05$). A stronger interaction between HACC and SA chains might be responsible for the improved mechanical properties of the PU/HACC/SA based NFDs. The multi-layer NFDs loading 2 % Rg3 depicted higher values of elongation, tensile strength and lower Young's modulus than the PU/HACC/SA based NFDs. This trend became obvious as the drug loading content was increased from 2 % to 4 %, implying that the small molecular drug, Rg3 might modulate the mechanical properties of the NFDs. Overall, the newly developed scaffolds had sufficient mechanical strength to protect the burn wounds and prevent tearing during their transport and storage (Liu et al., 2018).

3.4. Water absorption and water vapor transmission rates

An ideal wound dressing should effectively absorb the excess wound exudate and provide a moist healing environment for the wounds (Porrelli et al., 2021). The absorption abilities of the wound exudate of various NFDs were assessed by examining their water absorption rates (WARs) (Fig. 2B). The WAR values of the PU/HACC and PU/SA based NFDs was significantly higher as compared to the pure PU based NFDs ($p < 0.05$). The polysaccharides such as SA and HACC in the composite NFDs could form gels after the water absorption, leading to their excellent WAR values (Abasalizadeh et al., 2020). The PU/HACC/SA based NFDs presented the highest WAR among all the dressings, which could be owing to the existence of two different marine polysaccharides, producing synergistic gels upon water absorption (Zhang et al., 2014). When the hydrophobic Rg3 molecules were loaded in the dressings, the WAR values of the corresponding NFDs were reduced relative to the drug-free composite NFDs. An optimal dressing should also possess adequate water vapor transmission rates (WVTRs) to ensure efficient gas exchange, minimal wound exudate accumulation and reduced risks of bacterial infections (Tarusha et al., 2018). It has been suggested that the WVTR values of a wound dressing should be within the range of 2000–2500 g•m^{-2}•day^{-1} (Queen et al., 1987). Pure PU based NFDs illustrated extremely high WVTR values (3481.14 g•m^{-2}•day^{-1}) (Fig. 2C). Interestingly, the polysaccharide (*i.e.*, HACC, SA) amalgamated and Rg3 loaded composite dressings demonstrated significantly declined WVTR values as compared to the pure PU based NFDs ($p < 0.05$). These conferred their beneficial characteristics of regulating the wound microenvironments.

3.5. Surface wettability

The water contact angles (WCAs) of various composite NFDs at different time points were captured and compared with that of pristine PU NFDs (Fig. 3A). The pure PU based NFDs demonstrated excellent wettability and were completely wetted within 10 s. The wettability of the NFDs was considerably influenced by the presence of HACC or SA. The WCA of the PU/SA based scaffolds was lower (10 S, 11.5°) than that of PU/HACC NFDs (10 S, 43.5°). The wettability of the PU/HACC/SA NFDs was in between PU/HACC and PU/SA dressings. The WCA of Rg3-

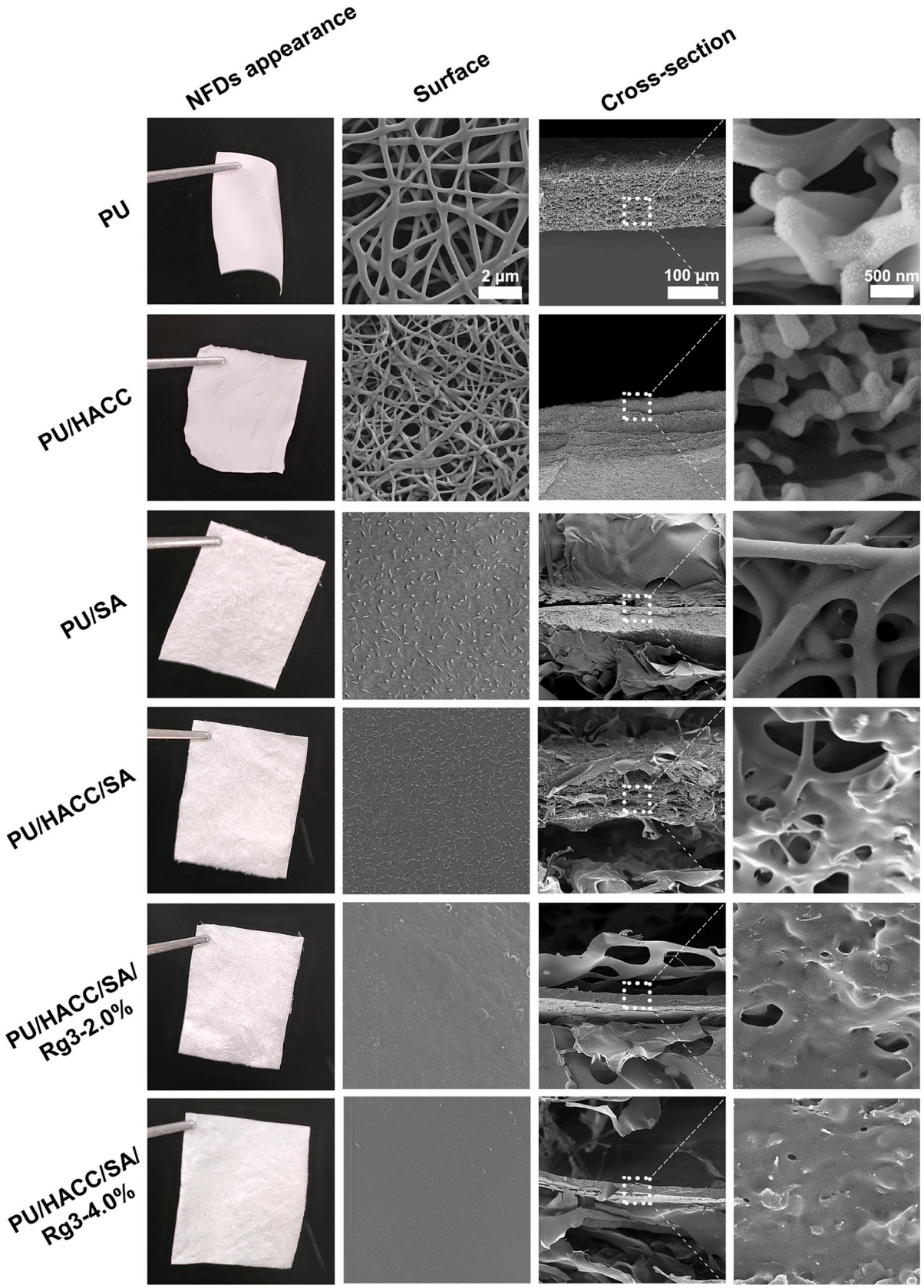

Fig. 1. The appearance of various NFDs and the SEM images of their surfaces and cross-sectional morphologies.

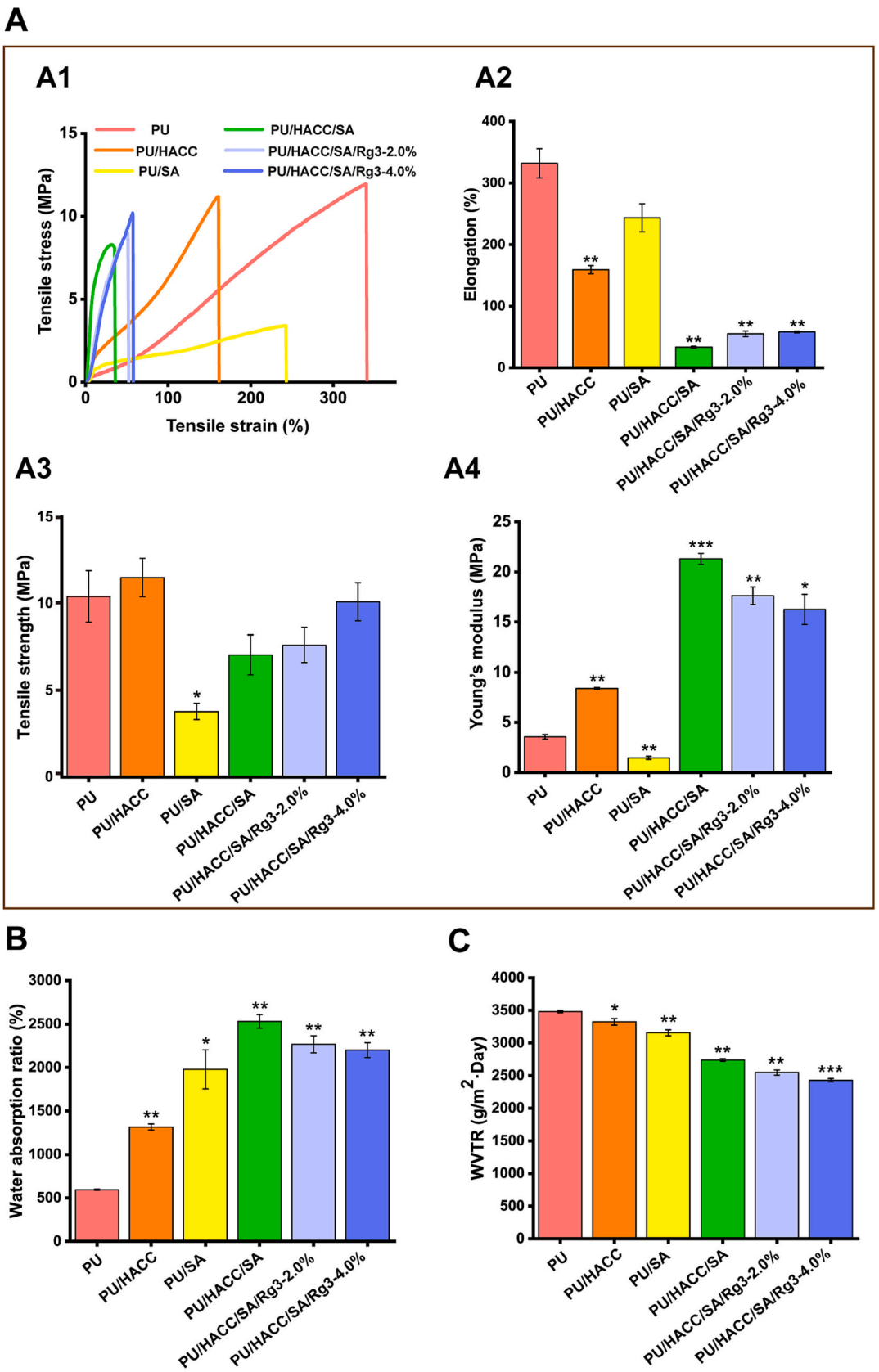

Fig. 2. The mechanical properties of NFDs (A) including their strain-stress curves (A1), ultimate strain (A2), ultimate tensile strength (A3) and Young's modulus (A4). The WARs (B) and WVTRs (C) of different NFDs. (*$p < 0.05$, **$p < 0.01$, ***$p < 0.001$, compared with PU).

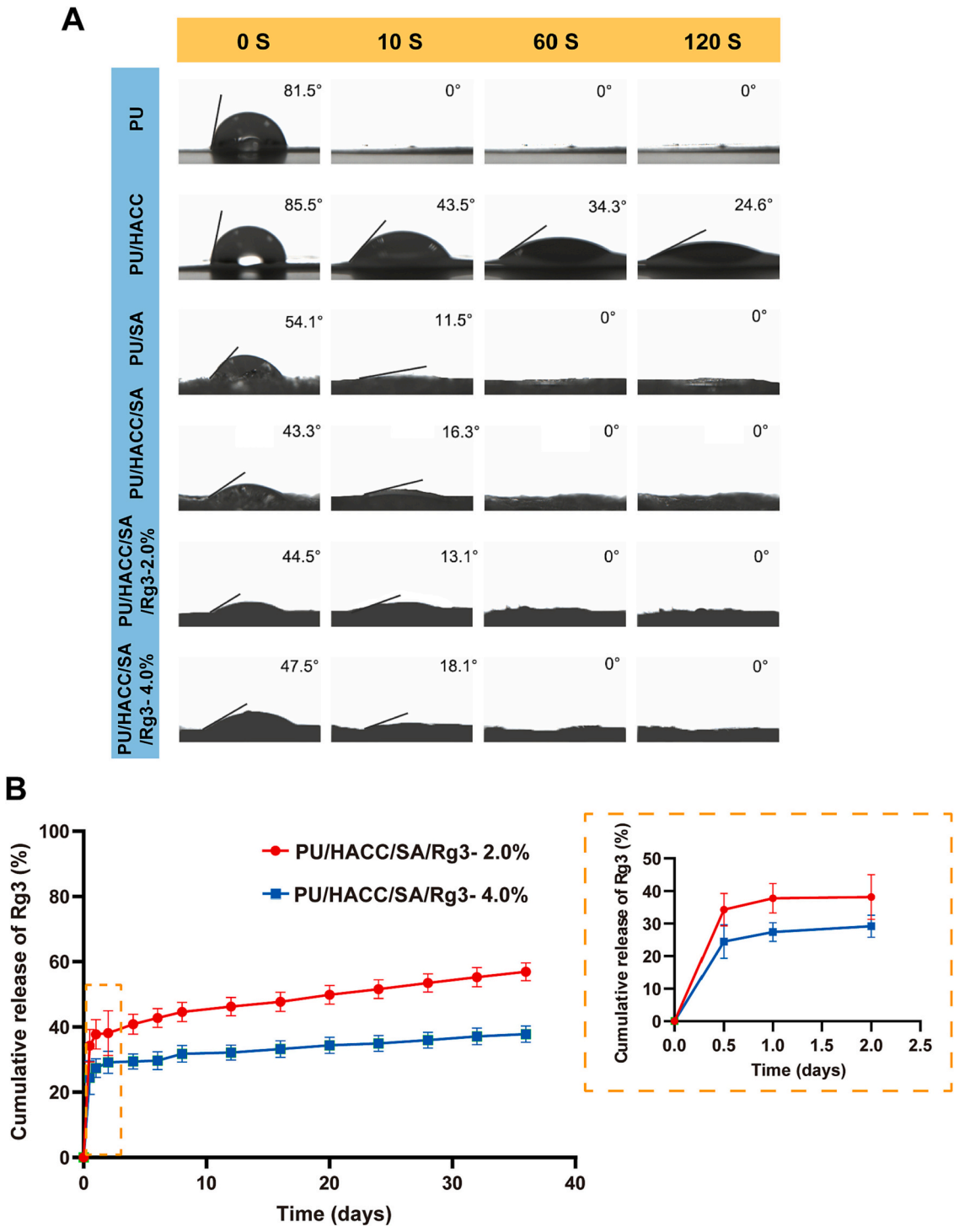

Fig. 3. The WCAs of different NFDs at variable time points (A) and the Rg3 release profiles of NFDs with time (B).

loaded NFDs did not significantly change as compared to PU/HACC/SA based NFDs. In general, various NFDs showed excellent wettability, which might be essential for fibroblast adhesion and their growth during the burn wound healing process.

3.6. Rg3 release behavior

The Rg3 release patterns of different PU/HACC/SA/Rg3 based NFDs were investigated under sink conditions of PBS (pH 7.4) and compared (Cheng et al., 2013). The PU/HACC/SA/Rg3 NFDs typically exhibited a bi-phasic drug release profile, demonstrating an initial fast release (within 1 day), followed by a slow diffusion controlled release phase up to 35 days (Fig. 3B). The initial fast drug release was related to the rapid dissolution or diffusion of surface associated Rg3 molecules of the NFDs. The second lower drug release rate stage could be attributed to the slower diffusion of the insoluble drug Rg3 inside the fibers from the non-biodegradable polyurethane matrix before diffusion into the bulk (Verreck et al., 2003). As the drug loading was increased from 2 % to 4 %, the Rg3 elution rates at both the early and late phases were reduced, owing to the difficulty in extravasation of the insoluble Rg3 molecules from the nanofibers. The Rg3 release profiles of NFDs were fitted into different release kinetic models. According to the results, the Rg3 elution

profiles of the multilayer dressings were primarily complied with Korsmyer-Peppas model (Table S3). The values of the release exponent ($n < 0.45$) indicated that the drug release mechanism was dominated by Fickian diffusion (Alimohammadi et al., 2022). The values of 'K_{kp}' declined with increasing Rg3 contents in NFDs. While the burn-wound healing potentials of NFDs at the cellular levels and in the animal model were investigated, we were primarily interested in comparing the efficacies of various polysaccharide-blended composite NFDs and eventually pure PU based NFDs were excluded from the following studies. On the other hand, the 2 % drug loaded composite dressings were selected for the cell and animal experiments based on the reported *in vivo* administered dose of Rg3 (Sun et al., 2014).

3.7. Cell proliferation, migration and adhesion

The cell proliferation effects of various NFDs were determined on NIH-3T3 and HaCat cells (Fig. 4A, B). The NFDs revealed no cytotoxicity at their low concentrations (0.5 %, v/v). As the concentration of PU/

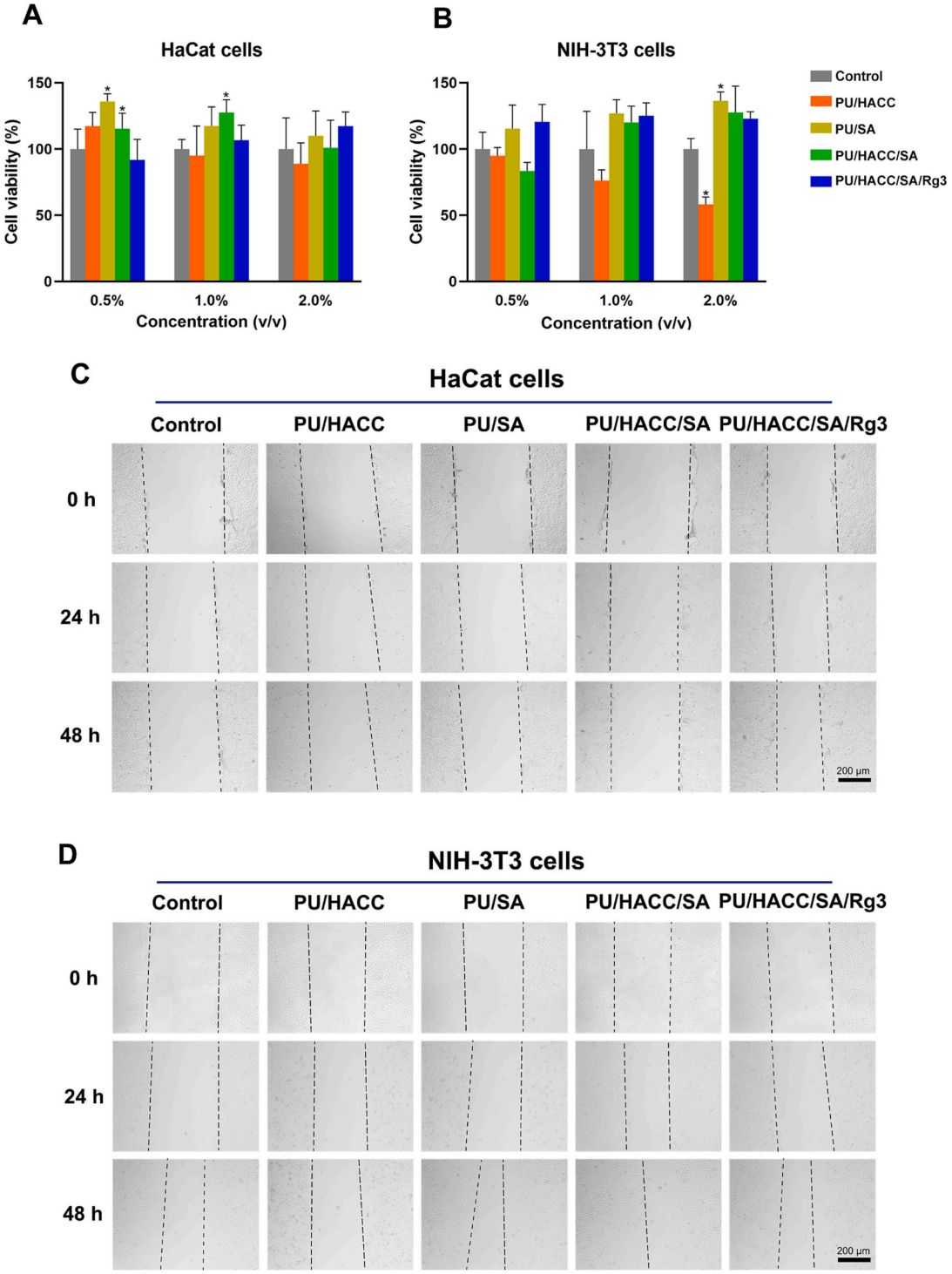

Fig. 4. The effects of different concentrations of NFD extracts on the proliferation of HaCat (A) and NIH-3T3 (B) cells. (*$p < 0.05$, compared with control). The impacts of NFD extracts on HaCat (C) and NIH-3T3 (D) cell migration.

HACC scaffolds was increased from 1.0 % to 2.0 %, a notable growth inhibition effects on keratinocytes and fibroblasts were evidenced. On contrary, the PU/SA dressings possessed an obvious growth promotion potential on these cells. Interestingly, PU/HACC/SA based NFDs also exhibited cell growth promoting effects. The cytotoxic activity of PU/HACC based scaffolds could be attributed to the electrostatic interactions between the negatively charged cells and the positively charged amino groups of HACC chains (J.-K. Lee et al., 2002). While HACC was blended with SA in PU/HACC/SA based NFDs, the cationic HACC segments could interact with the anionic SA chains *via* strong electrostatic interactions, reducing their cytotoxic potentials (Borges et al., 2006). The drug-loaded NFDs (2.0 %) portrayed no significant effects on keratinocyte and fibroblast growths relative to the blank control group.

The effects of various NFDs on cell migration were further evaluated on HaCat and NIH-3T3 cells. As compared to the blank control group, the PU/HACC scaffolds did not obviously affect keratinocyte migration, whereas the PU/SA, PU/HACC/SA and PU/HACC/SA/Rg3 dressing treated groups notably promoted cell migration (Fig. 4C). This indicated that the scaffolds containing SA could promote the migration of keratinocytes, while Rg3 had no considerable effect on keratinocyte migration. The effects of different NFDs on the migration of NIH-3T3 cells were also investigated (Fig. 4D). The PU/HACC dressing treated group showed a remarkable inhibitory effect on fibroblast migration relative to the control group, whereas the PU/SA scaffolds promoted fibroblast migration. The PU/HACC/SA NFDs also facilitated a significant NIH-3T3 cell migration. This signified that the combination of two marine polysaccharides (*viz.,* HACC and SA) could significantly promote the fibroblast migration. The Rg3-loaded scaffold treated group promoted the fibroblast migration at a considerably slower rate than that of PU/HACC/SA NFDs. Fig. S8 depicted the adhesion abilities of fibroblasts on various composite NFDs. The fibroblasts could adhere and grow on these composite scaffolds, indicating that the NFDs were extremely compatible with these cells.

3.8. *In vivo deep burn wound healing potentials*

We successfully established a third-degree burn wound rat model. According to the H&E staining results (Fig. S9), it proved that utilizing an 18 s burn time was appropriate. For shorter burn times (12 s), some portions of the dermis layer still remained. Conversely, increasing the burn time over 20 s, would result in partial destruction of the muscle layers. The animals treated with fabricated NFDs and their *in vivo* therapeutic properties were assessed *via* different experimental protocols (Fig. 5A). The rats treated with Sorbalgon®, an alginate based microfibrous dressing, was chosen as positive control in our study. All the scaffolds were cut into 22.0 mm circles and adhered to the burn wounds. After debridement, silicone rings with an inner diameter of 31.0 mm were fixed around the burn wounds (Fig. 5B) (Y. Li, Zhang, et al., 2022).

The macroscopic changes of wounds as a function of time were shown in Fig. 5C and D. The animal skins turned white with obvious blisters immediately after the development of deep third-degree burn wounds, which was consistent with the clinical symptoms of deep burn injuries (Petrone et al., 2014). After 21 days of treatment, the color of the regenerate skins and the size of the unhealed wound area of the PU/HACC/SA, PU/HACC/SA/Rg3, and Sorbalgon® treated groups was remarkably improved as compared to other scaffold treated groups. The wound closure rates of different animal groups were analyzed over variable time points (Fig. 5E). There were no significant differences in the rates of wound closure among various groups in the early stage of wound healing (7 days). This was because the contraction of the rodent wounds in the initial period was restricted in the presence of the silicone rings. The inhibitory effects of HACC on the proliferation of epidermal cells and fibroblasts resulted in the slowest wound healing rates of PU/HACC scaffold treated group after 14 days as compared to the blank control and other NFDs treated groups. After 21 days of treatment, different scaffold (except PU/HACC based NFDs) treated animals demonstrated significantly enhanced wound closure rates than that of the control group ($p < 0.05$). Interestingly, the wound closure rate of the PU/HACC/SA/Rg3 group was closer to that of the PU/HACC/SA scaffold and Sorblgon® treated groups implying that loaded Rg3 molecules in the multilayer dressings had no obvious effects on burn wound healing. According to our findings, when two polysaccharides were combined in NFDs, these could generate synergistic therapeutic effects and reverse the negative impacts of HACC residues in wound healing. As shown in Fig. 5F, the trends in body weight changes of the animals in each group were extremely similar during the experiment, indicating their good health conditions in the healing period.

3.9. *H&E staining of wound tissues*

Following treatment, the wound healing potentials of different dressings were further investigated through H&E staining of wound tissues at variable time points (Fig. 6A). Initially, the deep third-degree burns resulted in the destruction of the entire dermis, including appendages such as hair follicles and sebaceous glands. After 7 days of treatment, the loose granulation tissues of various groups were in an intensive inflammatory state due to the infiltration of both neutrophils and monocyte/macrophages (marked by open squares) (Watts et al., 2006). The inflammation could be observed even after 14 days, but the epidermis layers began to spread in each group (illustrated by black solid lines). After 21 days, the inflammation of the PU/HACC treated group and control group was still obvious and their epidermis crawling rates were slower than other groups. It could be attributed to their cationic chitosan residues, which could stimulate the immune activities and inhibit the proliferation of keratinocytes (Jou, 2011; Sayın et al., 2008). An enhanced wound healing effects of PU/HACC/SA/Rg3, PU/HACC/SA based NFDs and the commercial dressing, Sorblgon® might be related to their high moisture absorption and retention properties, which were beneficial in maintaining a moist healing environment of skins (Yang et al., 2011).

3.10. *Collagen deposition at the wound sites*

To assess the efficacy of different NFDs on burn wound healing, the deposition of total collagen and ratios of collagen I and III at the wound sites were further explored using Masson trichrome staining and Picrosirius Red (PSR) staining, respectively. The collagen fibers were stained in blue, while the muscle fibers were spotted in red following Masson's trichrome staining of wound tissues (GU et al., 2022). The PU/HACC/SA and PU/HACC/SA/Rg3 treated groups displayed denser collagen deposition than that of control and other composite scaffold treated groups after 21 days (Fig. 7A). Furthermore, the deposited collagens of PU/HACC/SA/Rg3 treated group were matured in nature, which resembled with the normal skins. It is noteworthy that the immature collagens are deposited as filaments (black arrows), whereas the dense matured collagens are often deposited in a basket weave pattern (yellow arrows) (Molavi, 2017). The composite NFDs loaded with Rg3 could regulate the collagen synthesis of fibroblasts and reveal a promising effect in preventing the formation of excessive scars (Sun et al., 2014).

Different types of collagen deposition in the wound tissues were also quantified using Sirius red staining protocol. When the stained wound tissue specimens were examined under a polarizing microscope, type I collagen appeared in yellow or red, and type III collagen was evidenced in green (Castleberry et al., 2016). After 14 days of treatment, the collagen I/III ratios of the control, PU/HACC and PU/SA treated groups were significantly higher than those in normal skin, while the collagen I/III ratios of PU/HACC/SA, PU/HACC/SA/Rg3 and positive control groups were similar to that of healthy skin tissues. It has been reported that collagen III would transform into collagen I during the wound

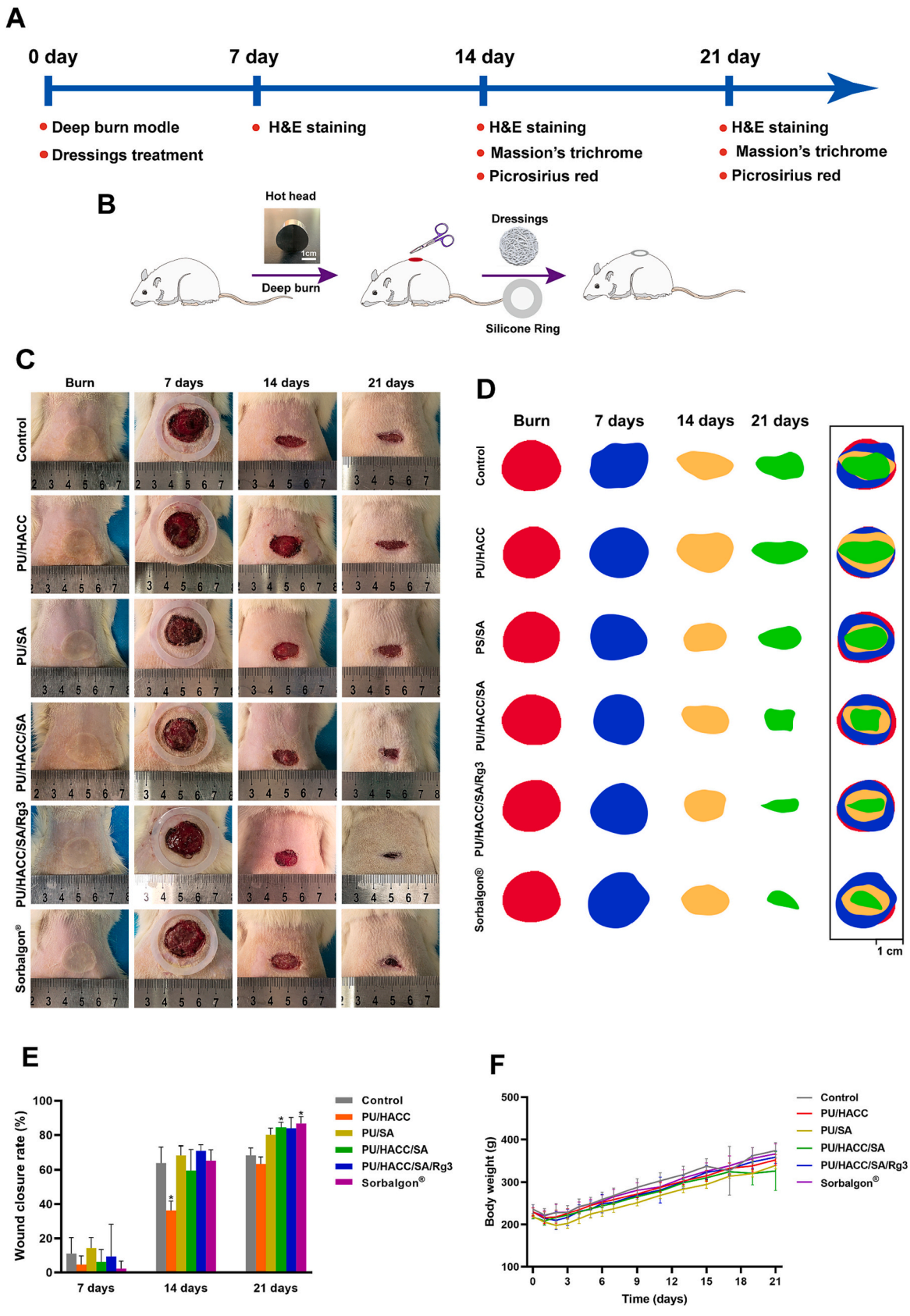

Fig. 5. Various experimental protocols for evaluating the wound healing potentials of NFDs on third-degree burn rat models (A). The development of third-degree burn rat models and the application of NFDs on the burn wounds (B). Representative macroscopic appearances of wounds during their healing process (C) and simulation plots of wounds (D) of different animal groups treated with various NFDs and the commercial Sorbalgon® over time. Wound closure rates of various groups (E) (*$p < 0.05$, compared with the control group). The curves of body weight changes of each group of animals during the experiment (F).

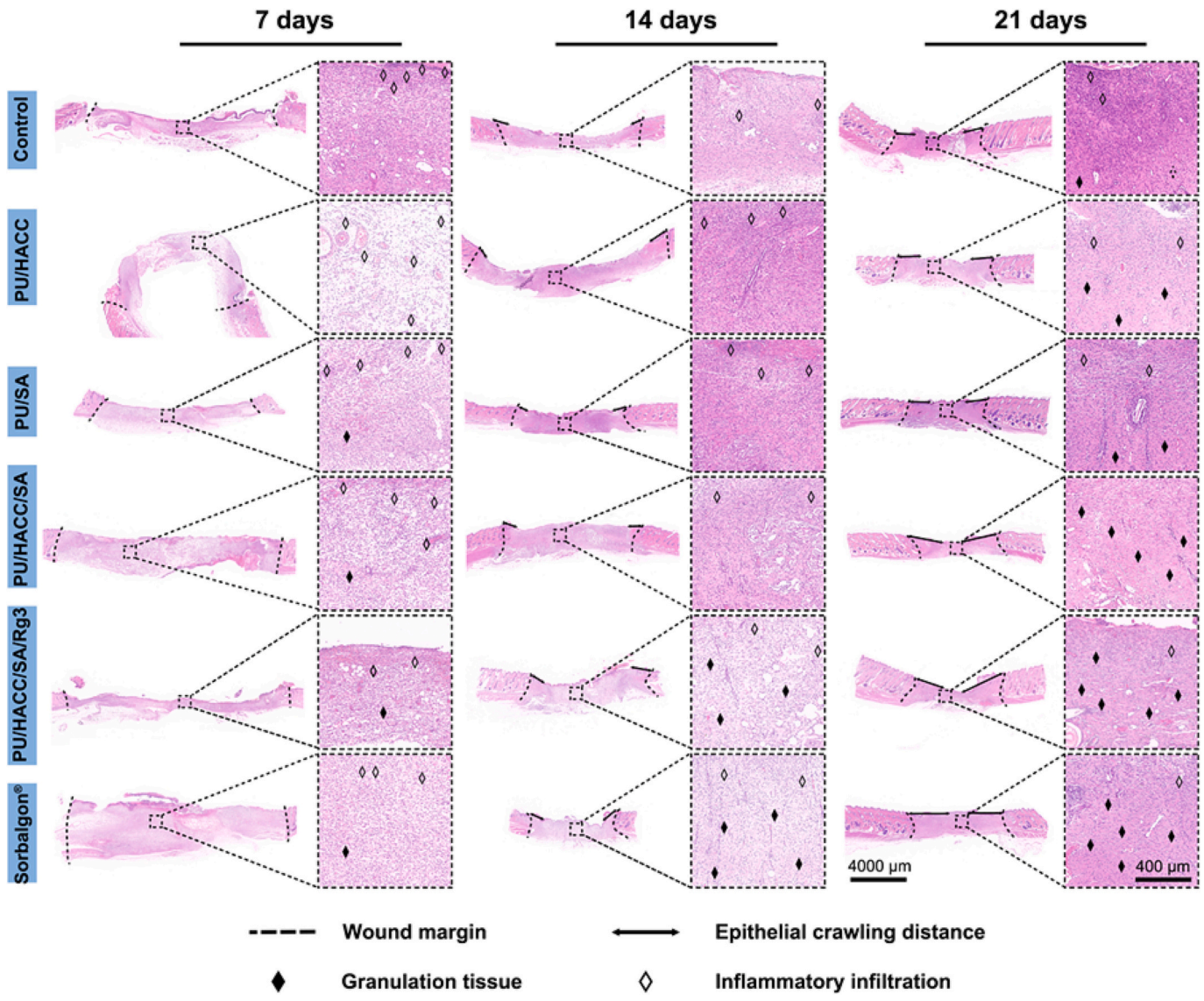

Fig. 6. H&E staining images of different groups treated with NFDs, demonstrating their wound healing potentials over time.

healing process, which could promote tissue maturation at the wound sites, but abnormal collagen deposition might lead to the formation of hypertrophic scars (Slemp & Kirschner, 2006). The PU/HACC/SA/Rg3 scaffold treated groups also displayed collagen I/III ratios closer to that of normal skins even after 21 days of treatment. This implied that the Rg3-loaded NFDs were efficient in regulating the ratios of type I and III collagens in the healing tissues, eliciting their beneficial effects in reducing excessive scars.

3.11. *Angiogenesis at the wound sites*

Angiogenesis is a critical process in the wound tissue regeneration (Luo et al., 2021). The extent of angiogenesis at the wound sites in each group was assessed by dual immunofluorescence staining of CD31 and α-SMA after 21 days of treatment (Fig. 8). Platelet endothelial cell adhesion molecule (CD31) is a pivotal marker of the endothelial cells of the blood vessels, whereas α-smooth muscle actin (α-SMA) is mainly expressed in the muscular layer of the mature blood vessels (Zhao et al., 2021). The angiogenesis in the new tissues could be confirmed when CD31 and α-SMA were spotted in red, and green color, respectively. The appearance of mature blood vessels in the PU/HACC/SA and PU/HACC/SA/Rg3 treated groups were similar to that of the marketed Sorbalgon® group (green arrow), while other groups showed more immature small blood vessels (red arrows). These results clearly demonstrated that the composite NFDs containing both HACC and SA could improve the blood vessel regeneration at the wound sites.

4. Conclusions

In our current research endeavors, various NFDs composed of synthetic polymer (*i.e.,* PU), marine-derived polysaccharides (*viz.,* HACC and SA), and Rg3 were successfully fabricated using the electrospinning and freeze-drying technologies. The PU/HACC/SA and PU/HACC/SA/Rg3 based NFDs exhibited favorable physicochemical properties and improved therapeutic potentials in deep burn wound management as compared to other composite NFDs (PU/HACC, PU/SA). Precisely, PU/HACC/SA and PU/HACC/SA/Rg3 NFDs could promote keratinocyte and fibroblast proliferation and their migration. The PU/HACC/SA and PU/HACC/SA/Rg3 based NFDs could also remarkably improve burn wound healing potentials in the animal model by accelerating epidermal closure, reducing inflammation, and promoting blood vessel maturation at the wound sites. Furthermore, PU/HACC/SA/Rg3 could prevent the formation of scars by regulating the collagen I/III ratios at the wound sites, which were similar to that of healthy skins. Thus, the research

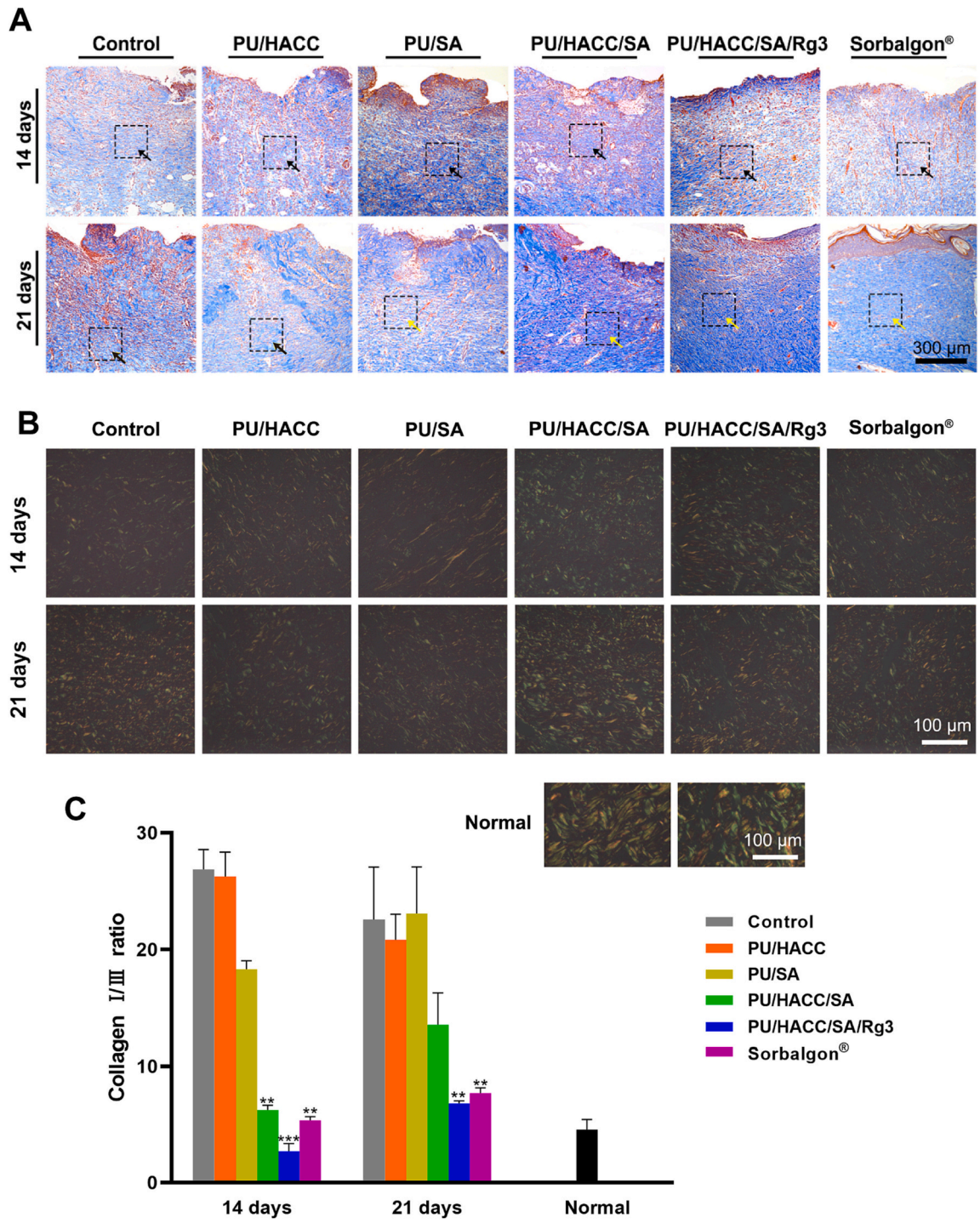

Fig. 7. Representative tissue images of Masson trichrome staining, revealing the collagen deposition after 14 and 21 days of treatment (black arrows represented immature collagen, while yellow arrows showed mature collagen) (A). Representative photographs of collagen fibers stained with Picrosirius red (PSR) after 14 and 21 days of therapy (B). Quantitative analyses of the collagen I/III ratios of various groups treated with NFDs and Sorbagon®(C).

hypotheses of our studies were proven true. Overall, this study demonstrated that the newly developed NFDs comprising PU, HACC, SA and Rg3 could exert effective healing activities on deep burn wounds with improved wound curing aesthetics.

CRediT authorship contribution statement

Xiong Guo: Conceptualization, Methodology, Validation, Writing – original draft. **Fangfang Xiu:** Methodology, Validation. **Hriday Bera:** Writing – review & editing. **Yasir Faraz Abbasi:** Writing – review & editing. **Yang Chen:** Investigation, Methodology. **Liangwei Si:** Investigation, Methodology. **Peixin Liu:** Investigation, Methodology. **Chunwei Zhao:** Investigation, Methodology. **Xing Tang:** Writing – review & editing. **Yu Feng:** Writing – review & editing. **Dongmei Cun:** Supervision, Writing – review & editing. **Xia Zhao:** Supervision, Writing – review & editing. **Mingshi Yang:** Conceptualization, Supervision, Writing – review & editing, Project administration, Funding acquisition.

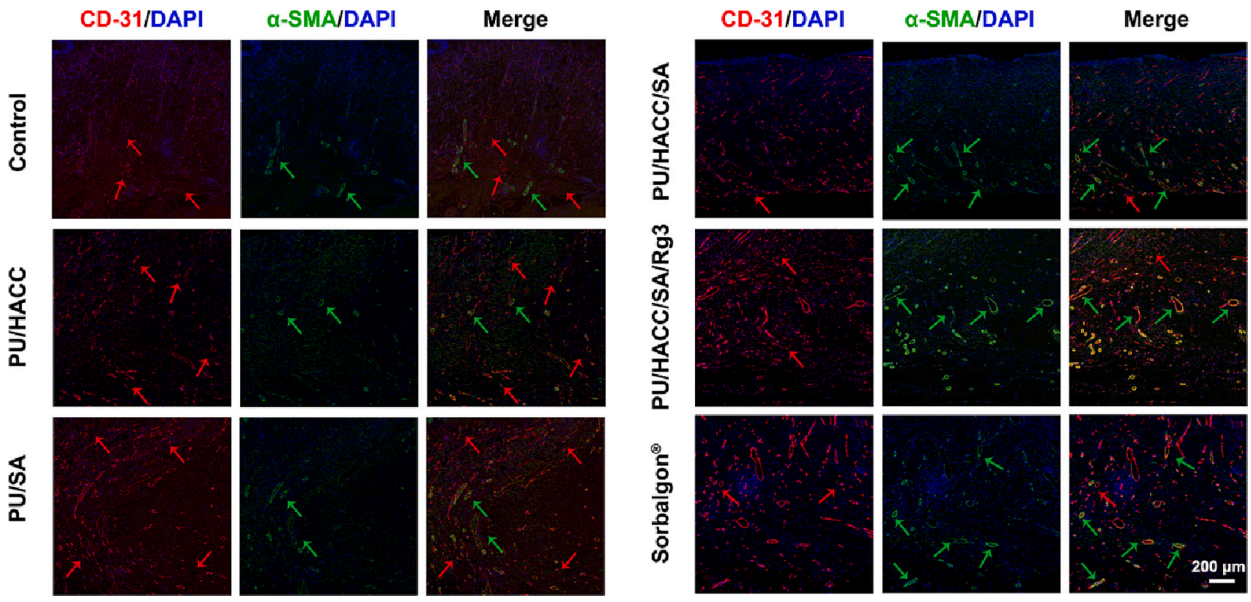

Fig. 8. The images of wound tissues after dual immunofluorescence staining of α-SMA and CD31, displaying the extent of angiogenesis in different groups treated with various NFDs and Sorbagon®.

Declaration of competing interest

The authors declare no competing financial interest.

Data availability

Data will be made available on request.

Acknowledgements

This work was financially supported by the Liaoning Pan Deng Xue Zhe Scholar (No. XLYC2002061), the National Natural Science Foundation of China (No. 82173768), and the Overseas Expertise Introduction Project for Discipline Innovation ("111 Project") (No. D20029). X. G. acknowledges the Educational Department of Liaoning Province (grant No. LJKZ0925), (Youth Project, grant No. LJKQZ2021035), the international postdoctoral exchange fellowship program (grant No. PC2021047) and Liaoning Provincial Doctoral Research Start-Up Fund (grant No. 2023-BS-110). H. B. thanks the financial support from National Natural Science Foundation of China (grant No. 82050410448) and Fellowship of China Postdoctoral Science Foundation (grant No. 2021MD703857). D.Cun acknowledges financial support from the General Project of Science and Technology Research Project of Liaoning Province (No. 2022-MS-241), and Ministry of Education Chunhui Program (2020).

Appendix A. Supplementary data

Supplementary data to this article can be found online at https://doi.org/10.1016/j.carbpol.2023.121085.

References

Abasalizadeh, F., Moghaddam, S. V., Alizadeh, E., Kashani, E., Fazljou, S. M. B., Torbati, M., & Akbarzadeh, A. (2020). Alginate-based hydrogels as drug delivery vehicles in cancer treatment and their applications in wound dressing and 3D bioprinting. *Journal of Biological Engineering, 14*(1), 1–22.

Aghmiuni, A. I., Keshel, S. H., Sefat, F., & AkbarzadehKhiyavi, A. (2021). Fabrication of 3D hybrid scaffold by combination technique of electrospinning-like and freeze-drying to create mechanotransduction signals and mimic extracellular matrix function of skin. *Materials Science and Engineering: C, 120*, Article 111752.

Alimohammadi, M., Fakhraei, O., Moradi, A., Kabiri, M., Moradi, A., Passandideh-Fard, M., … Mousavi Shaegh, S. A. (2022). Controlled release of azithromycin from polycaprolactone/chitosan nanofibrous membranes. *Journal of Drug Delivery Science and Technology, 71*, Article 103246.

Alipour, S. M., Nouri, M., Mokhtari, J., & Bahrami, S. H. (2009). Electrospinning of poly (vinyl alcohol)–water-soluble quaternized chitosan derivative blend. *Carbohydrate Research, 344*(18), 2496–2501.

Alvarez, X., Alves, A., Ribeiro, M. P., Lazzari, M., Coutinho, P., & Otero, A. (2021). Biochemical characterization of Nostoc sp. exopolysaccharides and evaluation of potential use in wound healing. *Carbohydrate Polymers, 254*, Article 117303.

Aoyagi, S., Onishi, H., & Machida, Y. (2007). Novel chitosan wound dressing loaded with minocycline for the treatment of severe burn wounds. *International Journal of Pharmaceutics, 330*(1–2), 138–145.

Atiyeh, B. S., Hayek, S. N., & Gunn, S. W. (2005). New technologies for burn wound closure and healing—Review of the literature. *Burns, 31*(8), 944–956.

Bagheri, M., Validi, M., Gholipour, A., Makvandi, P., & Sharifi, E. (2022). Chitosan nanofiber biocomposites for potential wound healing applications: Antioxidant activity with synergic antibacterial effect. *Bioengineering & translational medicine, 7*(1), Article e10254.

Borges, O., Cordeiro-da-Silva, A., Romeijn, S. G., Amidi, M., de Sousa, A., Borchard, G., & Junginger, H. E. (2006). Uptake studies in rat Peyer's patches, cytotoxicity and release studies of alginate coated chitosan nanoparticles for mucosal vaccination. *Journal of Controlled Release, 114*(3), 348–358.

Castleberry, S. A., Almquist, B. D., Li, W., Reis, T., Chow, J., Mayner, S., & Hammond, P. T. (2016). Self-assembled wound dressings silence MMP-9 and improve diabetic wound healing in vivo. *Advanced Materials, 28*(9), 1809–1817.

Cheng, L., Sun, X., Hu, C., Jin, R., Sun, B., Shi, Y., … Zhang, Y. (2013). In vivo inhibition of hypertrophic scars by implantable ginsenoside-Rg3-loaded electrospun fibrous membranes. *Acta Biomaterialia, 9*(12), 9461–9473.

Dos Santos, D. M., Correa, D. S., Medeiros, E. S., Oliveira, J. E., & Mattoso, L. H. (2020). Advances in functional polymer nanofibers: From spinning fabrication techniques to recent biomedical applications. *ACS Applied Materials & Interfaces, 12*(41), 45673–45701.

Fan, Q., Miao, C., Huang, Y., Yue, H., Wu, A., Wu, J., … Ma, G. (2021). Hydroxypropyltrimethyl ammonium chloride chitosan-based hydrogel as the split H5N1 mucosal adjuvant: Structure-activity relationship. *Carbohydrate Polymers, 266*, Article 118139.

Farokhi, M., Mottaghitalab, F., Fatahi, Y., Khademhosseini, A., & Kaplan, D. L. (2018). Overview of silk fibroin use in wound dressings. *Trends in Biotechnology, 36*(9), 907–922.

GU, P., BS, U., MG, A., Mohan, D., Pillai, K., .R., & TT, S. (2022). Electrospun polysaccharide scaffolds: Wound healing and stem cell differentiation. *Journal of Biomaterials Science, Polymer Edition, 33*(7), 858–877.

Guo, X., Liu, Y., Bera, H., Zhang, H., Chen, Y., Cun, D., … Yang, M. (2020). α-Lactalbumin-based nanofiber dressings improve burn wound healing and reduce scarring. *ACS Applied Materials & Interfaces, 12*(41), 45702–45713.

Gupta, A., Kowalczuk, M., Heaselgrave, W., Britland, S. T., Martin, C., & Radecka, I. (2019). The production and application of hydrogels for wound management: A review. *European Polymer Journal, 111*, 134–151.

Iacob, A.-T., Drăgan, M., Ionescu, O.-M., Profire, L., Ficai, A., Andronescu, E., … Lupaşcu, D. (2020). An overview of biopolymeric electrospun nanofibers based on polysaccharides for wound healing management. *Pharmaceutics, 12*(10), 983.

Jou, C.-H. (2011). Antibacterial activity and cytocompatibility of chitosan-N-hydroxy-2,3-propyl-N methyl-N,N-diallylammonium methyl sulfate. *Colloids and Surfaces B: Biointerfaces, 88*(1), 448–454.

Khan, F. A., Butt, A. U. R., Asif, M., Ahmad, W., Nawaz, M., Jamjoom, M., & Alabdulkreem, E. (2020). Computer-aided diagnosis for burnt skin images using deep convolutional neural network. *Multimedia Tools and Applications, 79*(45), 34545–34568.

Lee, J.-K., Lim, H.-S., & Kim, J.-H. (2002). Cytotoxic activity of aminoderivatized cationic chitosan derivatives. *Bioorganic & Medicinal Chemistry Letters, 12*(20), 2949–2951.

Lee, K. Y., & Mooney, D. J. (2012). Alginate: Properties and biomedical applications. *Progress in Polymer Science, 37*(1), 106–126.

Li, H., Ziemer, M., Stojanovic, I., Saksida, T., Maksimovic-Ivanic, D., Mijatovic, S., … Krajnovic, T. (2022). Mesenchymal stem cells from mouse hair follicles reduce hypertrophic scarring in a murine wound healing model. *Stem Cell Reviews and Reports*, 1–17.

Li, L., Wang, Y., Guo, R., Li, S., Ni, J., Gao, S., … Fan, G. (2020). Ginsenoside Rg3-loaded, reactive oxygen species-responsive polymeric nanoparticles for alleviating myocardial ischemia-reperfusion injury. *Journal of Controlled Release, 317*, 259–272.

Li, Y., Shen, Q., Shen, J., Ding, X., Liu, T., He, J., … Zhu, J. (2021). Multifunctional fibroblasts enhanced via thermal and freeze-drying post-treatments of aligned electrospun nanofiber membranes. *Advanced Fiber Materials, 3*(1), 26–37.

Li, Y., Zhang, X., He, D., Ma, Z., Xue, K., & Li, H. (2022). 45S5 Bioglass® works synergistically with siRNA to downregulate the expression of matrix metalloproteinase-9 in diabetic wounds. *Acta Biomaterialia, 145*, 372–389.

Liu, X., Nielsen, L. H., Kłodzińska, S. N., Nielsen, H. M., Qu, H., Christensen, L. P., … Yang, M. (2018). Ciprofloxacin-loaded sodium alginate/poly (lactic-co-glycolic acid) electrospun fibrous mats for wound healing. *European Journal of Pharmaceutics and Biopharmaceutics, 123*, 42–49.

Luo, M., Wang, M., Niu, W., Chen, M., Cheng, W., Zhang, L., … Leng, T. (2021). Injectable self-healing anti-inflammatory europium oxide-based dressing with high angiogenesis for improving wound healing and skin regeneration. *Chemical Engineering Journal, 412*, Article 128471.

Min, T., Zhu, Z., Sun, X., Yuan, Z., Zha, J., & Wen, Y. (2020). Highly efficient antifogging and antibacterial food packaging film fabricated by novel quaternary ammonium chitosan composite. *Food Chemistry, 308*, Article 125682.

Miranda, C. S., Silva, A. F. G., Pereira-Lima, S. M., Costa, S. P., Homem, N. C., & Felgueiras, H. P. (2022). Tunable spun fiber constructs in biomedicine: Influence of processing parameters in the fibers' architecture. *Pharmaceutics, 14*(1), 164.

Molavi, D. W. (2017). *The practice of surgical pathology: A beginner's guide to the diagnostic process*. Springer.

Moon, S., Ryu, B. Y., Choi, J., Jo, B., & Farris, R. J. (2009). The morphology and mechanical properties of sodium alginate based electrospun poly (ethylene oxide) nanofibers. *Polymer Engineering & Science, 49*(1), 52–59.

Noor, A., Afzal, A., Masood, R., Khaliq, Z., Ahmad, S., Ahmad, F., … Irfan, M. (2022). Dressings for burn wound: A review. *Journal of Materials Science*, 1–37.

Peng, Z.-X., Wang, L., Du, L., Guo, S.-R., Wang, X.-Q., & Tang, T.-T. (2010). Adjustment of the antibacterial activity and biocompatibility of hydroxypropyltrimethyl ammonium chloride chitosan by varying the degree of substitution of quaternary ammonium. *Carbohydrate Polymers, 81*(2), 275–283.

Periayah, M. H., Halim, A. S., & Saad, A. Z. M. (2016). Chitosan: A promising marine polysaccharide for biomedical research. *Pharmacognosy Reviews, 10*(19), 39.

Petrone, P., Asensio, J. A., & Marini, C. P. (2014). Management of accidental hypothermia and cold injury. *Current Problems in Surgery, 51*(10), 417–431.

Porrelli, D., Gruppuso, M., Vecchies, F., Marsich, E., & Turco, G. (2021). Alginate bone scaffolds coated with a bioactive lactose modified chitosan for human dental pulp stem cells proliferation and differentiation. *Carbohydrate Polymers, 273*, Article 118610.

Queen, D., Gaylor, J., Evans, J., Courtney, J., & Reid, W. (1987). The preclinical evaluation of the water vapour transmission rate through burn wound dressings. *Biomaterials, 8*(5), 367–371.

Sayın, B., Somavarapu, S., Li, X. W., Thanou, M., Sesardic, D., Alpar, H. O., & Şenel, S. (2008). Mono-N-carboxymethyl chitosan (MCC) and N-trimethyl chitosan (TMC) nanoparticles for non-invasive vaccine delivery. *International Journal of Pharmaceutics, 363*(1), 139–148.

Slemp, A. E., & Kirschner, R. E. (2006). Keloids and scars: A review of keloids and scars, their pathogenesis, risk factors, and management. *Current Opinion in Pediatrics, 18*(4).

Sofi, H. S., Abdal-hay, A., Ivanovski, S., Zhang, Y. S., & Sheikh, F. A. (2020). Electrospun nanofibers for the delivery of active drugs through nasal, oral and vaginal mucosa: Current status and future perspectives. *Materials Science and Engineering: C, 111*, Article 110756.

Sun, X., Cheng, L., Zhu, W., Hu, C., Jin, R., Sun, B., … Cui, W. (2014). Use of ginsenoside Rg3-loaded electrospun PLGA fibrous membranes as wound cover induces healing and inhibits hypertrophic scar formation of the skin. *Colloids and Surfaces B: Biointerfaces, 115*, 61–70.

Tang, M., Bian, W., Cheng, L., Zhang, L., Jin, R., Wang, W., & Zhang, Y. (2018). Ginsenoside Rg3 inhibits keloid fibroblast proliferation, angiogenesis and collagen synthesis in vitro via the TGF-β/Smad and ERK signaling pathways. *International Journal of Molecular Medicine, 41*(3), 1487–1499.

Tarusha, L., Paoletti, S., Travan, A., & Marsich, E. (2018). Alginate membranes loaded with hyaluronic acid and silver nanoparticles to foster tissue healing and to control bacterial contamination of non-healing wounds. *Journal of Materials Science: Materials in Medicine, 29*(2), 1–14.

Ulset, A.-S. T., Mori, H., Dalheim, M.Ø., Hara, M., & Christensen, B. E. (2014). Influence of amino acids, buffers, and pH on the γ-irradiation-induced degradation of alginates. *Biomacromolecules, 15*(12), 4590–4597.

Unnithan, A. R., Barakat, N. A., Pichiah, P. T., Gnanasekaran, G., Nirmala, R., Cha, Y.-S., … Kim, H. Y. (2012). Wound-dressing materials with antibacterial activity from electrospun polyurethane–dextran nanofiber mats containing ciprofloxacin HCl. *Carbohydrate Polymers, 90*(4), 1786–1793.

Verreck, G., Chun, I., Rosenblatt, J., Peeters, J., Van Dijck, A., Mensch, J., … Brewster, M. E. (2003). Incorporation of drugs in an amorphous state into electrospun nanofibers composed of a water-insoluble, nonbiodegradable polymer. *Journal of Controlled Release, 92*(3), 349–360.

Wang, Y., Beekman, J., Hew, J., Jackson, S., Issler-Fisher, A. C., Parungao, R., … Maitz, P. K. (2018). Burn injury: Challenges and advances in burn wound healing, infection, pain and scarring. *Advanced Drug Delivery Reviews, 123*, 3–17.

Watts, J. A., Zagorski, J., Gellar, M. A., Stevinson, B. G., & Kline, J. A. (2006). Cardiac inflammation contributes to right ventricular dysfunction following experimental pulmonary embolism in rats. *Journal of Molecular and Cellular Cardiology, 41*(2), 296–307.

Xiong, J., Liu, Y., Li, A., Wei, L., Wang, L., Qin, X., & Yu, J. (2021). Mass production of high-quality nanofibers via constructing pre-Taylor cones with high curvature on needleless electrospinning. *Materials & Design, 197*, Article 109247.

Yang, J.-S., Xie, Y.-J., & He, W. (2011). Research progress on chemical modification of alginate: A review. *Carbohydrate Polymers, 84*(1), 33–39.

Zhang, C., Chen, J.d., & Yang, F.-q. (2014). Konjac glucomannan, a promising polysaccharide for OCDDS. *Carbohydrate Polymers, 104*, 175–181.

Zhao, J., Patel, J., Kaur, S., Sim, S.-L., Wong, H. Y., Styke, C., … Khosrotehrani, K. (2021). Sox9 and Rbpj differentially regulate endothelial to mesenchymal transition and wound scarring in murine endovascular progenitors. *Nature Communications, 12*(1), 2564.

Zheng, S., Xie, Y., Li, Y., Li, L., Tian, N., Zhu, W., … Hu, H. (2014). Development of high drug-loading nanomicelles targeting steroids to the brain. *International Journal of Nanomedicine, 9*, 55.